This is a preprint, the final version is subject to change, of the American Mineralogist (MSA)
Cite as Authors (Year) Title. American Mineralogist, in press.
(DOI will not work until issue is live.) DOI: http://dx.doi.org/10.2138/am.2014.4676

Ms. 4676 – Revision 1

Rates of Li diffusion in garnet: Coupled transport of Li and Y+REEs

RYAN C. CAHALAN*, ERIC D. KELLY, WILLIAM D. CARLSON

Department of Geological Sciences, University of Texas at Austin, Austin, Texas 78712, U.S.A.

Short Title: Li diffusion in garnet

ABSTRACT

Numerical simulation of stranded diffusion profiles in partially resorbed garnet crystals from the aureole of the Makhavinekh Lake Pluton (Labrador, Canada) yields quantitative rates of intracrystalline diffusion for Li in garnet. Diffusion coefficients for Li at 700–900 °C and 0.53 GPa are 0.5–1.5 $\log_{10}$ units lower than those for divalent cations in the same samples, and match those for Y and Yb. This correspondence likely stems from coupled substitution of Li and Y (or REE) ions in the garnet structure: the requirement of local electroneutrality limits Li mobility to be no faster than that of Y+REEs. Because of this coupling, Li zoning in garnet is retained to comparatively high temperatures, making garnet a valuable monitor of the behavior of Li in deep crustal systems.

Keywords: Lithium, yttrium, REEs, garnet, intracrystalline diffusion, coupled substitution

INTRODUCTION

The uptake and diffusional redistribution of Li in rocks from a variety of geologic settings has proven to be an effective monitor of fluid-rock and melt-rock interactions, and intracrystalline diffusion of Li, along with diffusion-induced isotopic fractionation, offers insights into the kinetics of these processes (e.g., Tomascak et al. 2000; Zack et al. 2003; Coogan et al. 2005; Magna et al. 2006a; Ionov & Seitz 2008; Dohmen et al. 2010; Penniston-Dorland et al. 2010, 2012; Charlier et al. 2012; Richter et al. 2014). In several minerals, intracrystalline diffusional homogenization of Li occurs very rapidly at low temperatures (e.g., plagioclase: Giletti and Shanahan 1997; clinopyroxene: Coogan et al. 2005; quartz: Charlier et al. 2012); other minerals are partially retentive, but only up to mid-crustal temperatures (e.g., olivine: Dohmen et al. 2010; zircon: Cherniak and Watson 2010). Thus identification of host phases that are more highly resistant to Li diffusion is essential to development of robust high-temperature geochemical recorders of Li systematics.

This study investigates rates of Li diffusion in garnet, extracting quantitative diffusivities for Li from partially resorbed crystals by means of numerical simulation of the evolution of stranded diffusion profiles at their rims. It documents restricted mobility of Li — at rates indistinguishable from the rates of diffusion of Y and Yb — that is inferred to result from coupling of the diffusive fluxes of Li to those of Y+REEs, as a means of preserving local charge balance for Li within the garnet structure.

BACKGROUND AND PREVIOUS WORK

Little is known about Li zoning in garnet — and virtually nothing is known of its diffusivity — owing largely to the difficulty of measuring its low concentration at high spatial resolution before the advent of laser-ablation inductively coupled plasma mass spectrometry

(LA-ICPMS). The potential for determining Li diffusivity in natural garnet was suggested by recent work (Carlson 2012) in which the diffusivities of Y, REEs, and Cr, present at sub-ppm to hundreds-of-ppm levels, were extracted from stranded diffusion profiles measured by continuous LA-ICPMS scans, and were shown to be consistent with available experimental determinations at similar and higher temperatures. This study employs the same materials and closely similar methods, as abstracted in brief here; full details may be found in Carlson (2012).

Granulite-grade metapelites in the aureole of the Makhavinekh Lake Pluton (MLP) of northern Labrador (Canada) developed nearly homogeneous trace-element distributions in garnet during long residence at high temperatures in the deep crust (McFarlane et al. 2003; Kelly et al. 2011; Carlson, 2012). The rocks later were subjected to contact metamorphism at modest pressure (0.53 GPa) that produced peak temperatures ranging from ~900 °C near the contact to ~700 °C at distances of 4-5 km from it (McFarlane et al. 2003; Carlson 2006). These conditions rendered garnet unstable, and incomplete reaction in the nearly anhydrous aureole generated coronal reaction zones dominated by cordierite + orthopyroxene with accessory monazite (McFarlane et al. 2005), enclosing relict garnets whose rims developed stranded diffusion profiles (SDPs). These SDPs are gradients in concentration reflecting diffusional modifications in response to rim compositions that approached local equilibrium with the immediately adjacent coronal assemblage during reaction. Partitioning favorable to garnet produced outward increases in concentrations of Mn, Fe, Y, Cr, and REEs from Gd to Lu; partitioning favorable to the coronal product assemblage produced outward decreases in concentrations of Mg, Ca, Nd, Sm, and Eu.

Extraction of diffusivities from these SDPs relies on numerical simulation of their evolution. Calculated profiles that coincide closely with measured profiles emerge from a model

of multicomponent diffusion in a sphere undergoing resorption while partitioning elements between its outermost rim and its external environment. The model requires as input: an initial concentration profile; values for the pre-exponential constant and the activation energy in Arrhenius expressions for the tracer diffusion coefficients for each of the diffusing components; the variation of temperature with time during the resorption/diffusion event; and the activation energy for intergranular diffusion of the component that is rate-limiting for the diffusion-controlled resorption reaction. Except for the intracrystalline diffusion parameters (in this case, those for Li), which are the unknowns that are iteratively adjusted to produce congruence between measured and modeled profiles, all of these quantities are well-constrained within the MLP aureole (Carlson 2012, p. 1601-1602).

Application of this approach by Carlson (2012) to obtain diffusivities of Y, REEs, and Cr included detailed analysis of the precision and reproducibility of the results, as well as a sensitivity analysis that considered effects of uncertainties in the measured profiles and in values chosen for the input parameters (p. 1603-1605). Those analyses indicated that determination of a diffusion coefficient from an individual profile is precise to within ~ ±0.1 $\log_{10}$ unit, and reproducible across multiple samples to within ±0.40 $\log_{10}$ units on average; the diffusivities obtained from the SDPs were reconciled with reliable experimental data to within ±0.55 $\log_{10}$ units (at 95% confidence levels), an important demonstration of the validity of the approach.

METHODS

In this study, we adopt an approach nearly identical to that of Carlson (2012), with slight modifications to the sample-preparation procedure that were necessary for proper measurement of the SDPs for Li.

Four samples of the Tasiuyak Gneiss were chosen from a traverse oriented roughly perpendicular to the contact of the MLP (McFarlane et al. 2003); all four were also analyzed by Carlson (2012). These samples (M05, M20, M21, and M22) span the inner, higher-temperature portion of the aureole; map locations appear in Figure 2 of Carlson (2010). Samples from the outer, lower-temperature portion of the aureole yielded diffusion profiles with widths (< 5 μm) too narrow for accurate measurement of profiles. All SDPs were measured on central sections through garnet crystals, precisely located by high-resolution X-ray computed tomography (HRXCT). The HRXCT imagery was also used to select crystals that are nearly equant and isolated from neighboring porphyroblasts, to ensure that they approximate the spherical geometry used in the modeling. Profiles were located to avoid the influence of any pre-resorption fractures within the crystals.

Sample preparation: Acid leaching of grain-boundary Li

Initial examination of trace-element distributions in samples from the MLP aureole revealed, within most but not all grain boundaries, elevated Li concentrations on the order of 10-100 times greater than peak concentrations within the garnet: a grain-boundary "Li-spike". These spikes, which vary in their intensity and apparent width, degrade measurements of stranded diffusion profiles for Li in the garnet rims. It was therefore necessary to develop a protocol for removal of Li from the grain boundaries while preserving Li concentrations in garnet.

Reasoning that Li in the grain boundaries was likely hosted by late-stage, cryptocrystalline minerals more soluble than garnet, we sought to remove it by means of acid leaching. A series of tests using a variety of acids and concentrations was designed to assess different acids' ability to remove Li from the grain boundaries without altering the garnet chemistry. Table 1 provides a list of the acid-leaching methods tested without success as well as

the final method utilized in this study. Concentrated hydrofluoric acid (HF) is the only acid tested that successfully removed Li from the grain boundary. Further testing was conducted to confirm that no appreciable amount of Li is leached from the garnet during this process. This validation required a primary core-to-rim LA-ICPMS scan of garnet, extending a short distance into the surrounding matrix, followed by HF leaching over the scanned area. A pair of secondary scans was run after the leaching, one directly over the primary scan and the other adjacent and parallel to the primary scan, offset laterally by ~ 5 μm. Figure 1 presents some of these results, demonstrating the effectiveness of HF leaching of the grain boundary without alteration of the garnet chemistry. The optimized leaching technique implemented in this study involved a single 12 μl droplet of 40% HF applied directly onto the target grain boundary. This reaction progressed at atmospheric conditions for ~30 minutes, followed by rinsing with distilled water.

LA-ICPMS measurements of SDPs

To measure diffusion profiles along core-to-rim traverses in relict MLP garnet crystals, continuous laser ablation scans were performed using a 193 nm New Wave UP193FX fast-excimer laser system with an ESI/New Wave large-format laser cell. The flow path for sample extraction from the cell is localized just above the ablation pit, which minimizes washout times and increases spatial resolution. Instead of a circular laser spot, these analyses used a 5x50 μm rectangular slit, aligned with its long dimension perpendicular to the direction of the analytical traverse and parallel to the edge of the crystal, in order to achieve the required levels of spatial resolution and signal intensity.

Each analytical traverse was made at a scan rate of 1 μm/s at 20% laser power and a shot frequency of 10 Hz, using NIST 612 glass as a calibration standard and ^{29}Si as the internal standard for ablation-volume corrections. All measurements were taken as rim-core-rim

traverses, yielding symmetrical profiles with respect to the garnet center. An Agilent 7500ce ICPMS instrument was used to measure time-resolved analyte intensities for the gas blank and ablation intervals. For each traverse, ^{7}Li, ^{89}Y, and ^{172}Yb concentrations were measured, as well as ^{90}Zr and ^{47}Ti, which aid in identifying the presence of submicroscopic mineral inclusions in the analyzed profiles. Raw count rates were processed using the visualization and mass-spectrometric data-processing software IOLITE (Paton et al. 2011). Y and Yb profiles were measured to obtain well-defined positions for garnet edges, and to provide estimates of diffusivities that could be compared directly to the results of Carlson (2012) for verification of the protocols used in this study.

Convolution effects due to spot size and washout delays spread the signal in time and distance along the traverse; deleterious effects are most pronounced at the discontinuity represented by the edge of the crystal. These artifacts were removed using the deconvolution method described by Carlson (2012, p. 1617). All measured profiles presented here — and all profiles used in the fitting of numerical simulations — are the smoothed profiles produced by the deconvolution procedure.

Numerical simulations

Input parameters for the simulations were determined by the same means as in Carlson (2012): initial garnet profiles were extrapolated from unaffected interiors; thermal histories were derived from previously published 2-D conductive thermal models for the aureole; and a value of 265 kJ/mol (Carlson 2010) was used for the activation energy for intergranular diffusion of Al, as the rate-limiting control on the resorption reaction.

No prior estimates exist for the activation energy for Li diffusion in garnet. Considering the obvious correlation between SDPs for Li and those for Y and Yb (Fig. 2), we chose for input

the zero-pressure activation energy and the activation volume determined for Y+REE diffusion by Carlson (2012), namely 295 kJ/mol at zero pressure, corresponding to 306 kJ/mol at 0.53 GPa, the pressure of the MLP intrusion. (Any other choice for this parameter, within reasonable bounds, would yield only negligible differences in the retrieved diffusivities, owing to the narrow range of temperature over which diffusion took place in these samples; cf. Carlson, 2012, p. 1605.) Having chosen this provisional activation energy for Li diffusion, the only remaining unknown parameter is the value for the corresponding pre-exponential frequency factor, and this was adjusted in each fit to obtain optimal congruence with the measured profile. Extracted diffusivities are completely insensitive to the small misfits that typically appear at the outermost garnet edge and at the position of innermost penetration of the diffusive effects (Fig. 2), but they are highly sensitive to the location of the inflection point marking the steepest portion of the SDP (Carlson 2012, p. 1604). Accordingly, simulations in this work optimized the fits to the central region of the SDPs.

RESULTS

Stranded diffusion profiles for Li, Y and Yb in relict garnet are progressively narrower with increasing distance from the intrusive contact with the MLP, consistent with measured trace-element SDPs in previous studies (Kelly et al. 2011; Carlson 2012). The profiles generally consist of flat to shallowly sloping interiors, transitioning to steeply increasing gradients at positions ~50-250 μm from the rims: this position defines an approximate 'penetration depth' for diffusive effects. Profiles for Li, Y, and Yb all share a similar shape and penetration depth at each sample distance.

Numerically simulated SDPs for Li, Y, and Yb closely replicate those measured in all four samples; Li and Y profiles for a single representative example are shown in Figure 2. Two

SDPs were measured and fit in each sample except M05C, which yielded three. Table 2 compiles the extracted diffusion coefficients. As in Carlson (2012, p. 1603), the precision of each individual determination of the diffusivity is ~ ±0.1 $\log_{10}$ unit, and reproducibility as represented by the standard error of the mean (Table 2) is < 0.4 $\log_{10}$ units. Retrieved Y and Yb diffusivities differ from the mean values obtained by Carlson (2012, his Table 2) in independent analyses of the same samples by only ±0.25 $\log_{10}$ units on average (maximum ±0.53), and all fall within the published limits of reproducibility for those prior determinations.

Diffusivities were extracted from polythermal histories, so on an Arrhenius diagram they define short line segments whose slope is predetermined by the choice of the provisional activation energy. For ease of comparison to other published data, the diffusion coefficients are reported at a single point along each such line segment, the point corresponding to the characteristic temperature T_C (cf. Carlson 2012, p. 1605). The Arrhenius diagram in Figure 3 plots, for each sample, the average value for the diffusivity and its standard error of the mean, at the characteristic temperature for that sample's thermal history.

As expected from the similarity of the positions of the inflection points in profiles for all three elements in each traverse, the three diffusion coefficients extracted from each sample are indistinguishable from one another within procedural uncertainty. Contributing to the robustness of this result is the fact that *relative* rates of diffusion are immune to any potential errors in absolute rates that might stem from uncertainties in input parameters or natural vagaries of the resorption process. The resulting $\log_{10} D^*$ values for Li range from -22.14 m^2/s at 845 °C to -23.36 m^2/s at 809 °C; these values are approximately 1.0-1.5 $\log_{10}$ units smaller than values for divalent cations in garnet (Carlson 2006) and are equivalent within uncertainty to the values for diffusion of Y and the REEs in garnet (Carlson 2012).

DISCUSSION

Li in garnet has received relatively little attention, and its diffusive behavior has been uncharacterized until now. In other minerals, however, measured Li diffusivities appear to delineate two categories of behavior: rapid diffusion occurs if the mineral structure permits movement of Li via an interstitial mechanism, but diffusion is substantially retarded when Li diffusion is coupled to movement of other ions (Fig. 4).

Both behaviors have been observed in quartz, in experiments near the alpha-beta quartz transition conducted by Sartbaeva et al. (2005). Studying Li diffusion driven by an electrical field gradient, these investigators observed (p. 1104) that "Li^+ ions penetrate the quartz crystals and travel freely through the crystallographic channels perpendicular to the *c*-axis," but found (p. 1105) only "short-range penetration of Al with Li into the quartz." The very rapid transport of Li in quartz reported by Verhoogan (1952) and confirmed by Charlier et al. (2012) is attributed to the interstitial transport mechanism.

In plagioclase (both albite and anorthite), similarly rapid diffusion of Li was described by Giletti and Shanahan (1997) and was likewise attributed (p. 17) to an interstitial mechanism. Coogan et al. (2005) measured high rates of Li diffusion in diopside; although they offered no explanation in terms of mechanism, it has been suggested subsequently that this finding, along with the fast diffusion of Li in plagioclase, "may be due to the presence and mobility of interstitial Li that is possible in these structures" (Zhang and Wright 2012, p. 37).

A hybrid case is described for olivine by Dohmen et al. (2010). In their experiments, they identify the simultaneous operation of both a faster interstitial mechanism of Li diffusion and a slower mechanism that proceeds via octahedral-site vacancies. They point out that many factors control the relative importance of these mechanisms to Li transport in nature, making it difficult

to generalize; nonetheless, they indicate (p. 289) that in most cases in nature the faster interstitial mechanism (Fig. 4, line 4) will not be activated for reasonable vacancy concentrations expected in olivine above 800 °C, which implies a modest retentivity for Li in olivine at lower temperatures (Fig. 4, line 6). Zhang and Wright (2012, p. 37) likewise concluded, from a suite of detailed *ab initio* simulations, that "Li diffusion [in forsterite] via a purely interstitial mechanism is highly unlikely," as "the olivine structure does not contain open and direct 'channels' that could facilitate interstitial migration". Their model predicts Li incorporation as bound interstitial-substitutional pairs, and describes Li diffusion via a complex interplay among motions of Li and Mg that combines Mg-Li exchange and a vacancy-assisted interstitial mechanism.

A picture very similar to that in olivine emerges from the experiments of Richter et al. (2014) on diffusion of Li in clinopyroxene. They used a two-species Li diffusion model, with fast-diffusing interstitial Li and very slow-diffusing Li in metal sites, to explain the variety of isotopic and concentration profiles observed in their experiments and in natural pyroxene. Both Dohmen et al. (2010) and Richter et al. (2014) found that the high mobility of a fast-diffusing interstitial species could produce a decoupling of the equilibration of isotopic and chemical gradients, although with different senses: whereas Dohmen et al. identified isotopic equilibration as the faster process in olivine, Richter et al. found the opposite in pyroxene.

Cherniak and Watson (2010) reported that diffusion of Li in zircon is slower than in other minerals, and declined to invoke an interstitial mechanism, noting significant differences from the case of Li diffusion in olivine, and stating (p. 387): "if there were migration along interstitials in zircon it would likely be considerably faster than our results indicate". Similarly, they resisted the proposal by Ushikubo et al. (2008) that Li is incorporated into and diffusionally stabilized in zircon as interstitial Li^{+} ions bound to $(Y+REE)^{3+}$ ions substituting for Zr^{4+}; although they

acknowledged that this could not be ruled out, they emphasized that they found no difference in Li diffusivity between experiments conducted using diffusant sources with and without REE. Oxygen vacancies were proposed as an alternative means of providing local charge balance for Li incorporation.

As detailed below, we infer from the equivalent diffusivities of Li, Y and Yb measured in this study that the low mobility of Li in garnet is a direct consequence of substitutions that link Li to Y+REEs in adjoining structural sites, imposing a requirement that their fluxes be directly coupled in order to preserve local electroneutrality in the structure.

An alternative: Low-*T* diffusion of Li?

Before proceeding further, we wish to consider (but immediately reject) an alternative origin for the Li SDPs that would be consistent with rapid Li diffusion. In light of the high mobility of Li in other silicates, it might be imagined that the profiles for Li developed independently of those for Y, via rapid diffusion at lower temperatures. In this scenario, the high concentration of Li in the grain boundaries would serve as a source for inward diffusion of Li that took place after resorption ceased. This possibility can be ruled out definitively: the distance that Li diffuses into the interior of a crystal, measured to the steepest point in its SDP, correlates directly with the extent of the resorption reaction — and in every case matches very closely the inward distance to the steepest points of the Y+REE profiles — making it evident that Li diffusion took place concurrently with the resorption reaction. This reasoning also leads to the conclusion that the Li spike at the grain boundary was deposited after resorption ceased, via some still-unidentified process.

Coupled transport of Li and Y+REEs

The precise correspondence between SDPs for Li and those for Y and Yb immediately suggests that the transport of Li through the garnet structure is linked directly to the transport of Y+REEs. Such a linkage would arise naturally if Li incorporation into the structure proceeded via a coupled substitution scheme in which Y^{3+} and trivalent REEs provide local charge balance for Li^{+} to maintain electroneutrality. Recent lattice-dynamics calculations by Carlson et al. (2014) confirm that such coupled substitution schemes are energetically favorable; that they are consistent with analytical and crystallochemical constraints on trace-element concentrations in natural garnet; and that defect-association energies are high enough to ensure coupling of defects even at high temperatures, yet low enough to permit the transient partial dissociation required for diffusive motion. We describe below two possible substitution schemes that would couple the diffusion of Li to that of Y+REEs. (In the following, "M" is used to represent one or more of Mg, Fe, Mn, and Ca, which typically occupy the eightfold sites in garnet as divalent cations; and all ionic radii referenced are from Shannon 1976.)

The first substitution scheme is analogous to the means of Na^{+} incorporation identified in natural garnet by Enami et al. (1995), in which the exchange vector [$NaYM_{-2}$] introduces a $Y_{1.5}Na_{1.5}Al_2Si_3O_{12}$ component. The ionic radius of $^{VIII}Li^{+}$ is smaller than that of $^{VIII}Na^{+}$ (0.92 Å vs. 1.18 Å), but it falls within the range of radii for the $^{VIII}M^{2+}$ ions (0.89 Å for $^{VIII}Mg^{2+}$ to 1.12 Å for $^{VIII}Ca^{2+}$). This makes possible Li incorporation via the exchange vector [$LiYM_{-2}$], introducing a $Y_{1.5}Li_{1.5}Al_2Si_3O_{12}$ component. The calculations of Carlson et al. (2014, their Fig. 2) show that the exchange free energy of the [$LiYM_{-2}$] substitution is in fact slightly lower than that of [$NaYM_{-2}$], confirming that this substitution should operate in nature to establish charge-balance for Li. Furthermore, in pyrope-almandine hosts, the pairing of $^{VIII}Li^{+}$ with $^{VIII}Y^{3+}$ or $^{VIII}REE^{3+}$ is

289 calculated to be among the most energetically favorable means of incorporating Y+REEs into
290 aluminosilicate garnet, again making the coupling of these elements highly likely.

291 A second potential substitution scheme is suggested by analogy to the means of Y
292 incorporation identified by Grew et al. (2010) in which the menzerite exchange vector
293 [$Y(Mg,Fe)M_{-1}Al_{-1}$] introduces a $Y_2M(Mg,Fe)_2Si_3O_{12}$ component. Considering that the ionic
294 radius of $^{VI}Li^{+}$ (0.76 Å) falls between those of $^{VI}Mg^{2+}$ (0.72 Å) and $^{VI}Fe^{2+}$ (0.78 Å), it seems
295 plausible that Li incorporation might also proceed via the exchange vector [$Y_2LiM_{-2}Al_{-1}$],
296 introducing a $Y_2MLiAlSi_3O_{12}$ component. Indeed Hanrahan et al. (2009b, p. 998) suggested that
297 Li could enter octahedral sites in non-majoritic garnet, although they did not identify the coupled
298 substitution that would be required for charge-balance. The defect-energy calculations of Carlson
299 et al. (2014, their Fig. 2), however, show that this substitution scheme is energetically
300 substantially more costly than the alternative described above, except perhaps in near-end-
301 member grossular. It is therefore less likely to have a significant impact on Li diffusion in
302 nature.

303 Parenthetically, we note that Hanrahan et al. (2009a) have proposed that Li incorporation
304 in crustal garnets might proceed via an exchange vector [$LiPM_{-1}Si_{-1}$], introducing a
305 $LiM_2Al_2PSi_2O_{12}$ component. We suspect that this substitution scheme is also energetically highly
306 disfavored, but even to the extent that such exchanges do occur, they are likely to contribute little
307 to the diffusional mobility of Li, considering the immobility of P in garnet, attested to by the
308 preservation of very sharp discontinuities in P concentration even in crystals heated sufficiently
309 to promote homogenization of Y+REE concentrations (e.g., Fig. 3a of McFarlane et al. 2005;
310 Ague and Eckert 2012, p. 847).

Preservation of local charge balance for Li by either of the first two substitutional schemes described above would necessitate that Li could migrate no faster than allowed by the diffusion of Y+REEs. We therefore conclude that charge-coupling of Li with Y+REEs is responsible for the measured equivalence of their diffusivities.

In that regard, we note that the lattice-dynamics calculations of Carlson et al. (2014) demonstrate that, at 1200 K, the free energies of fully dissociated Li-(Y+REE) defects are ~200 kJ/mol higher than associated defects in their minimum-energy configurations, indicating that Li^{+} will remain strongly associated with Y^{3+} or REE^{3+} to provide local charge compensation while these ions diffuse through the garnet structure at high temperature. Nonetheless, calculated energies for partially dissociated ion pairs—in which the charge-compensating ions are not in adjacent polyhedra but instead are in second-, third-, or fourth-nearest polyhedra—are higher by only about 10-30 kJ/mol than energies for nearest-neighbor ions; because the quantity *RT* is 10 kJ/mol at 1200 K, appreciable fractions of the defects could transiently adopt these higher-energy configurations, as is required for associated defects to migrate during diffusion as charge-coupled pairs.

Finally, because Y+REEs are present in the MLP garnets (and most others) at substantially higher concentrations than Li, additional charge-compensation schemes that do not involve Li are required for Y^{3+} and REE^{3+}. This is not at all unexpected: Carlson (2012) argues that the dominant substitutional scheme responsible for Y+REE incorporation in MLP garnets is a menzerite-type exchange [$Y(Mg,Fe)M_{-1}Al_{-1}$], and that mobility of Y+REEs is consequently limited primarily by the mobility of ^{VI}Al, which must be exchanged for Mg or Fe in octahedral sites to maintain local electroneutrality when Y+REEs move through the structure. Ultimately,

then, the diffusion of Li in garnet is tied—through its dependence on Y+REE mobility—to the diffusion of Al in the sublattice of octahedral sites.

Li partitioning between relict garnet and cordierite

Corroborating evidence for charge-coupled substitutions involving Li and Y+REEs comes from a comparison of Li concentrations in MLP garnet to those of the cordierite that dominates the coronal reaction zone produced by resorption: Li concentrations in the Y+REE-rich garnet rims are substantially higher than predicted by equilibrium partitioning between normal garnet compositions and cordierite, exactly as expected if Li uptake is linked to that of Y+REEs by a coupled substitution.

The analyses of Dutrow et al. (1986) indicate that equilibrium partitioning of Li in pelitic rocks will normally favor cordierite over garnet. Dutrow et al. (2011) quantified this partitioning: the ratio of their stated K_D values for staurolite/garnet (260) and staurolite/cordierite (1.30) yields a K_D for cordierite/garnet of 200. We therefore anticipated, prior to measurement, that SDPs for Li in MLP garnets would drop from interior values to lower concentrations near the garnet rims.

Because the opposite is observed, we analyzed Li concentrations in the cordierite that dominates the coronal reaction zones surrounding relict MLP garnet, using the same LA-ICPMS protocols described above, except that 50 μm spots were employed, rather than the slit aperture. Those analyses consistently yielded Li concentrations in the range 10-60 ppm. Measured concentrations in the outermost garnet rims are comparable, and thus far above the values of a few tenths of ppm or lower that might be expected from partitioning with co-existing cordierite in the absence of the highly elevated Y+REE concentrations found within the stranded diffusion profiles. Thus, the elevated Li concentrations in garnet rims are seen to be a consequence of the high concentrations of Y+REEs that build up in rims during resorption: if either of the proposed

charge-coupled Li-(Y+REE) substitutions is operating, the increase in Y+REEs in the garnet rims stabilizes Li there as well.

IMPLICATIONS

Because the diffusion coefficients for Li obtained in this study match those of Y so closely, application of the Y diffusivity expression of Carlson (2012, Eqn. 2) should provide a reliable estimate for Li diffusivity as well. Such applications, whenever possible, should also evaluate whether or not Li fluxes are related to the fluxes of Y+REEs, a key supposition following from these results. The potential for competing mechanisms involving high-mobility interstitial Li ions seems low, insofar as crystallochemical considerations militate against the likelihood of an appreciable population of interstitial ions in structures as compact as garnet. Nonetheless, given their importance in olivine and pyroxene, it would be prudent to maintain a watchful eye for possible effects of this kind in garnet as well.

The near-equivalence of diffusivities for Li and for Y and Yb found in this study strongly implies that coupled Li-(Y+REE) substitution governs the rate of Li diffusion in natural garnet, and—although independent confirmation would strengthen this inference—the intracrystalline diffusion of Li in garnet is seen here to be significantly slower than in other silicate minerals. The key implication of this finding is that Li zoning in garnet can record and retain evidence of high-temperature processes, even those occurring during metamorphism at or above the transition from amphibolite-facies to granulite-facies conditions, which has the potential to greatly expand the use of Li zoning in garnet as a monitor of fluid-rock (and melt-rock) interaction.

ACKNOWLEDGMENTS

Ben Byerly aided development of the leaching experiments, and Nate Miller guided LA-ICPMS data collection and reduction. Samples used in this study were collected by Chris McFarlane and Jim Connelly. Financial support was provided by NSF grant EAR-1144309 to WDC. We are grateful to Daniele Cherniak and Ralf Dohmen for insightful and helpful reviews.

REFERENCES CITED

Ague, J.J. and Eckert, D.E. (2012) Precipitation of rutile and ilmenite needles in garnet: Implications for extreme metamorphic conditions in the Acadian Orogen, U.S.A.. American Mineralogist, 97, 840-855.

Carlson, W.D. (2006) Rates of Fe, Mg, Mn, and Ca diffusion in garnet. American Mineralogist, 91, 1-11.

Carlson, W.D. (2010) Dependence of reaction kinetics on H_2O activity as inferred from rates of intergranular diffusion of aluminium. Journal of Metamorphic Geology, 28, 735-752.

Carlson, W.D. (2012) Rates and mechanism of Y, REE, and Cr diffusion in garnet. American Mineralogist, 97, 1598-1618.

Carlson, W.D., Gale, J.G., and Wright, K. (2014) Incorporation of Y and REEs in aluminosilicate garnet: Energetics from atomistic simulation. American Mineralogist, in press. DOI: 10.2138/am2014.4720

Charlier, B.L.A., Morgan, D.J., Wilson, C.J.N., Wooden, J.L., Allan, A.S.R., and Baker, J.A. (2012) Lithium concentration gradients in feldspar and quartz record the final minutes of magma ascent in an explosive supereruption. Earth and Planetary Science Letters, 319-320, 218-227.

Coogan, L.A., Kasemann, S.A. and Chakraborty, S. (2005) Rates of hydrothermal cooling of new oceanic upper crust derived from lithium-geospeedometry. Earth and Planetary Science Letters, 240, 415-424.

Cherniak, D.J. and Watson, E.B. (2010) Li diffusion in Zircon. Contributions to Mineralogy and Petrology, 160, 383-390.

Dohmen, R., Kasemann, S.A., Coogan, L., and Chakraborty, S. (2010) Diffusion of Li in olivine. Part I: Experimental observations and a multi species diffusion model. Geochimica et Cosmochimica Acta, 74, 274-292.

Dutrow, B.L., Holdaway, M.J., and Hinton, R.W. (1986) Lithium in staurolite and its petrologic significance. Contributions to Mineralogy and Petrology, 94, 496-506.

Dutrow, B.L., Miller, N.R., and Carlson, W.D. (2011) Lithium and trace-element incorporation into metapelitic minerals: new data from LA-ICP-MS measurements. Geological Society of America Abstracts with Programs, 43,150-151.

Enami, M., Cong, B., Yoshida, T., and Kawabe, I. (1995) A mechanism for Na incorporation in garnet: An example from garnet in orthogneiss from the Su-Lu terrane, eastern China. American Mineralogist, 80, 475-482.

Giletti, B.J. and Shanahan, T.M. (1997) Alkali diffusion in plagioclase feldspar. Chemical Geology, 139, 3-20.

Grew, E.S., Marsh, J.H., Yates, M.G., Lazic, B., Armbruster, T., Locock, A., Bell, S.W., Dyar, M.D., Bernhardt, H.J., and Medenbach, O. (2010) Menzerite-(Y), a new species, $\{(Y,REE)(Ca,Fe^{2+})_2\}[(Mg,Fe^{2+})(Fe^{3+},Al)](Si_3)O_{12}$, from a felsic granulite, Parry Sound, Ontario, and a new garnet end-member, $\{Y_2Ca\}[Mg_2](Si_3)O_{12}$. Canadian Mineralogist, 48, 1171-1193.

Hanrahan, M., Brey, G., Woodland, A., Altherr, R., and Seitz, H.M. (2009a) Towards a Li barometer for bimineralic eclogites: experiments in CMAS. Contributions to Mineralogy and Petrology, 158, 169-183.

Hanrahan, M., Brey, G., Woodland, A., Seitz, H.-M., and Ludwig, T. (2009 b) Li as a barometer for bimineralic eclogites: Experiments in natural systems. Lithos, 112S, 992-1001.

Ionov, D.A. and Seitz, H.-M. (2008) Lithium abundances and isotopic compositions in mantle xenoliths from subduction and intraplate settings: Mantle sources vs. eruption histories. Earth and Planetary Science Letters, 266, 316-331.

Kelly, E.D., Carlson, W.D., and Connelly, J.N. (2011) Implications of garnet resorption for the Lu-Hf garnet geochronometer: An example from the contact aureole of the Makhavinekh Lake Pluton, Labrador. Journal of Metamorphic Geology, 29, 901-916.

Magna, T., Wiechert, U., Grove, T.L. and Halliday, A.N. (2006a) Lithium isotope fractionation in the southern Cascadia subduction zone. Earth and Planetary Science Letters, 250, 428–443.

McFarlane, C.R.M., Carlson, W.D., and Connelly, J.N. (2003) Prograde, peak, and retrograde *P*-*T* paths from aluminium in orthopyroxene: High-temperature contact metamorphism in the aureole of the Makhavinekh Lake Pluton, Nain Plutonic Suite, Labrador. Journal of Metamorphic Geology, 21, 405-423.

McFarlane, C.R.M., Connelly, J.N., and Carlson, W.D. (2005) Monazite and xenotime petrogenesis in the contact aureole of the Makhavinekh Lake Pluton, northern Labrador. Contributions to Mineralogy and Petrology, 148, 524-541.

Paton, C., Hellstrom, J., Bence, P., Woodhead, J., and Hergt, J. (2011) Iolite: Freeware for the visualization and processing of mass spectrometric data. Journal of Analytical Atomic Spectrometry, 26, 2508-2518.

Penniston-Dorland, S.C., Sorensen, S.S., Ash, R.D., and Khadke, S.V. (2010) Lithium isotopes as a tracer of fluids in a subduction zone mélange: Franciscan Complex, CA. Earth and Planetary Science Letters, 292, 181–190.

Penniston-Dorland, S.C., Bebout, G.E., Pogge von Strandmann, P.A.E., Elliot, T., and Sorensen, S.S. (2012) Lithium and its isotopes as tracers of subduction zone fluids and metasomatic processes: Evidence from the Catalina Schist, California, USA. Geochimica et Cosmochimica Acta, 77, 530-545.

Richter, F., Watson, B., Chaussidon, M., Mendybaev, R., and Ruscitto, D. (2014) Lithium isotope fractionation by diffusion in minerals. Part 1: Pyroxenes. Geochimica et Cosmochimica Acta, 126, 352-370.

Sartbaeva, A., Wells, S.A., Redfern, S.A.T., Hinton, R.W., Reed, S.J.B. (2005) Ionic diffusion in quartz studied by transport measurements, SIMS and atomistic simulations. Journal of Physics: Condensed Matter,17, 1099-1112.

Shannon, R.D. (1976) Revised effective ionic radii and systematic studies of interatomic distances in halides and chalcogenides. Acta Crystallographica, A32, 751-767.

Tomascak, P.B., Ryan, J.G., and Defant, M.J. (2000) Lithium isotope evidence for light element decoupling in the Panama subarc mantle. Geology, 28, 507–510.

Ushikubo, T., Kita, N.T., Cavosie, A.J., Wilde, S.A., Rudnick, R.L., and Valley, J.W. (2008) Lithium in Jack Hills zircons: Evidence for extensive weathering of Earth's earliest crust. Earth and Planetary Science Letters, 272, 666-676.

Verhoogen, J. (1952) Ionic diffusion and electrical conductivity in quartz. American Mineralogist, 37, 637-655.

Zack, T., Tomascak, P. B., Rudnick, R. L., Dalpe´, C. and McDonough, W. F. (2003) Extremely light Li in orogenic eclogites: The role of isotope fractionation during dehydration in subducted oceanic crust. Earth and Planetary Science Letters, 208, 279– 290.

Zhang, F. and Wright, K. (2012) Lithium defects and diffusivity in forsterite. Geochimica et Cosmochimica Acta, 91, 32-39.

476

FIGURES

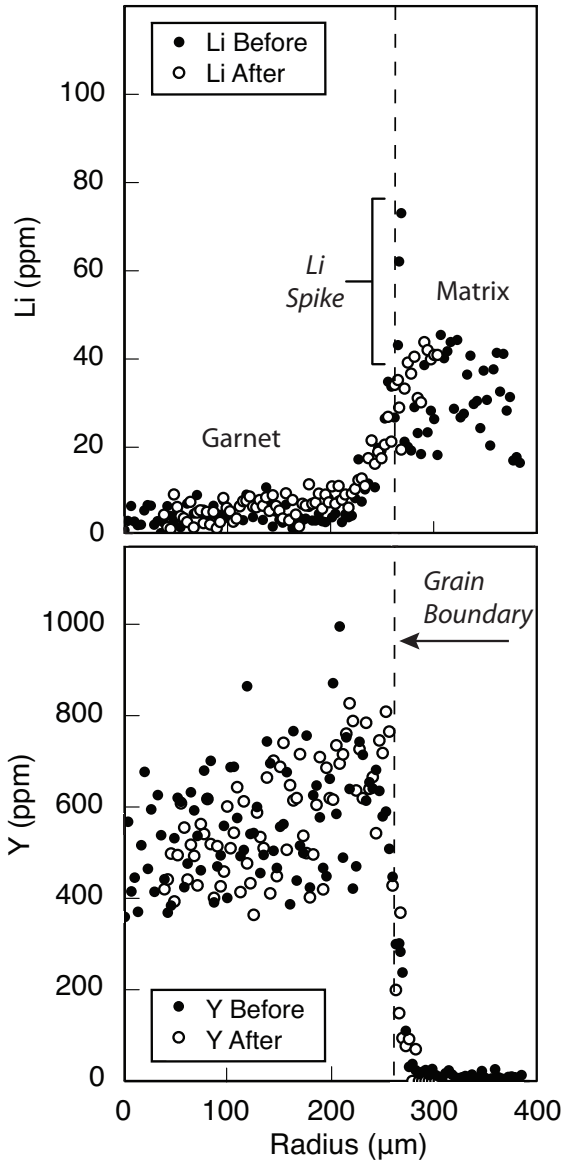

477

478 **FIGURE 1.**

479

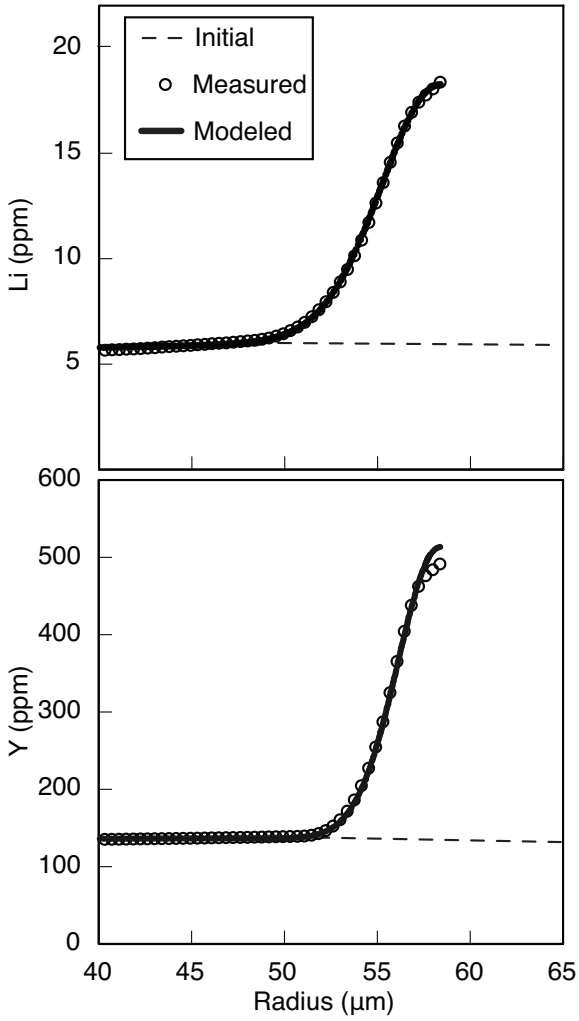

480

481 **FIGURE 2.**

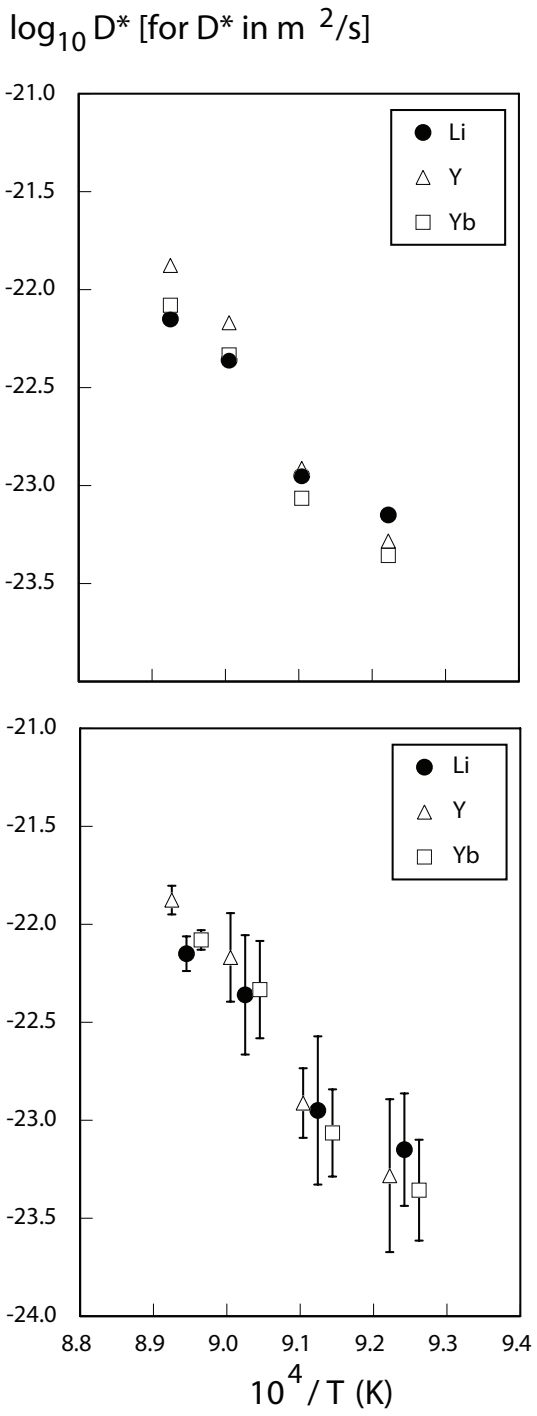

FIGURE 3.

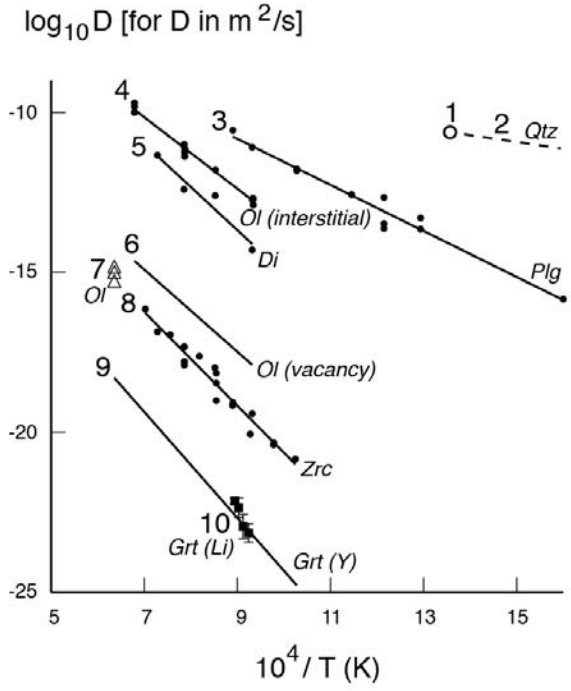

FIGURE 4.

Table 1. Acid-leaching tests

	HCl 2.3 M	HCl 12.1 M	H_2SO_4 18.0 M	HNO_3 15.9 M	$3HCl{\cdot}HNO_3$ 13.1 M	HF 28.9 M
Drop volume	Submerged	7 µL	7 µL	7 µL	7 µL	12 µL
Duration	20 h	2x 20 min	2x 20 min	2x 20 min	2x 20 min	20 min
Successful removal	no	no	no	no	no	yes

489

Table 2. Diffusivities extracted from stranded diffusion profiles

Sample	T_C (°C)	P (GPa)	$\log_{10} f_{O_2}$	n	Distance from MLP (m)	$\log_{10} D$*(std err) at T_C [for D in m^2/s]		
						Li	Y	Yb
M05	845	0.53	-17.46	3	800	-22.14(09)	-21.88(07)	-22.08(05)
M20	835	0.53	-17.63	2	1100	-22.36(30)	-22.17(26)	-22.33(25)
M21	823	0.53	-17.88	2	1500	-22.95(38)	-22.91(18)	-23.07(22)
M22	809	0.53	-18.23	2	2025	-23.15(29)	-23.28(39)	-23.36(26)

Notes: Diffusivities are mean values for all n determinations for each sample; uncertainties are standard errors of the mean, and apply to the two least-significant figures.

490

FIGURE CAPTIONS

FIGURE 1. Before-and-after leaching measurements demonstrate effective removal of the Li spike at the grain boundary without changing the internal chemistry of the MLP garnet. Example shown here is from a *non-central* garnet section, so Li and Y traverses exhibit only gentle rimward increases, rather than measurable stranded diffusion profiles. The excessive scatter seen in the Y concentrations is a result of preferential tuning of the ICPMS instrument to maximize sensitivity at low masses for Li analysis.

FIGURE 2. Example of measured and modeled SDPs for Li and Y from sample M21C1a. Note the close congruence of the Li and Y profiles, in particular the correspondence in location of the steepest portion, or inflection point, in each of the two profiles—a sensitive measure of each element's inward diffusive penetration. The view is restricted to the region near the rim of the relict garnet: measured profiles (*circles*) and modeled profiles (*solid line*) gradually rise further inward toward the garnet core at 0 μm, and initial profiles (*dashed line*) gently drop further outward toward original rim at 87 μm.

FIGURE 3. Arrhenius diagrams displaying Li, Y, and Yb diffusivity at each of four sampling distances. (*top*) Mean values, plotted at characteristic temperature T_C, which decreases with increasing distance from the intrusion. (*bottom*) Same data, with uncertainties. In each group, the points displayed represent a single temperature, although for clarity the Y and Yb points have been shifted ± 0.025 units in inverse temperature. Uncertainties are ± one standard error of the mean for each determination.

FIGURE 4. Diffusivity of Li in silicates. 1 = quartz (Charlier et al. 2012); 2 = quartz, extrapolation of low-*T* data of Verhoogen (1952); 3 = plagioclase (Giletti and Shanahan, 1997); 4 = olivine, interstitial mechanism (Dohmen et al. 2010); 5 = diopside (Coogan et al. 2005); 6 =

514 olivine, vacancy mechanism; 7 = olivine (Spandler and O'Neill 2010); 8 = zircon (Cherniak and
515 Watson 2010); 9 = Y diffusion in garnet (Carlson 2012); 10 = this study.